New early dark energy is compatible with current LSS data

Florian Niedermann[*] and Martin S. Sloth[†]

CP³-Origins, Center for Cosmology and Particle Physics Phenomenology,
University of Southern Denmark, Campusvej 55, 5230 Odense M, Denmark

Recently, a full-shape analysis of large-scale structure (LSS) data was employed to provide new constraints on a class of early dark energy models. In this paper, we derive similar constraints on new early dark energy (NEDE) using the publicly available PyBird code, which makes use of the effective field theory of LSS. We study the NEDE base model with the fraction of NEDE and the trigger field mass as two additional parameters allowed to vary freely, while making simplifying assumptions about the decaying fluid sector. Including the full-shape analysis of LSS together with measurements of the cosmic microwave background, baryonic acoustic oscillations, and supernovae data, we report $H_0 = 71.2 \pm 1.0 \text{ km s}^{-1} \text{ Mpc}^{-1}$ (68% C.L.) together with an approximate 4σ evidence for a nonvanishing fraction of NEDE. This is an insignificant change to the value previously found without full-shape LSS data, $H_0 = 71.4 \pm 1.0 \text{ km s}^{-1} \text{ Mpc}^{-1}$ (68% C.L.). As a result, while the NEDE fit cannot be improved upon the inclusion of additional LSS data, it is also not adversely affected by it, making it compatible with current constraints from LSS data. In fact, we find evidence that the effective field theory of LSS acts in favor of NEDE.

I. INTRODUCTION

Recent direct measurements of the expansion rate of the Universe using Type Ia supernovae as standard candles (SH$_0$ES [1]) are in tension with the expansion rate inferred form the cosmic microwave background (CMB) [2] when assuming the standard Λ cold dark matter (ΛCDM) cosmological model (for recent reviews, see Refs. [3–6]).[1] It is a hot subject of discussion whether unaccounted for systematical effects in astronomical distance measurements are responsible for this discrepancy or whether we have to refine our understanding of the history of the Universe by going beyond the ΛCDM model [9,10]. It turns out that cosmological measurements have reached a precision where modifying the history of the Universe to bring new concordance between CMB and direct measurements of the expansion rate is very difficult without introducing new tensions between different datasets. As theorists looking for a new concordance model to replace ΛCDM, we are truly experiencing that we have entered the era of precision cosmology. If we try to modify the late-time history to account for the higher value of H_0 measured

today by SH$_0$ES, then we quickly run into tension with baryon acoustic oscillation (BAO) measurements [3,4, 11–13]. On the other hand, an extra component of dark energy, which decays away shortly before recombination, has proved more promising as a possible solution [14–23]. The early dark energy (EDE) proposal suggests that the early dark energy is stored in a slow-rolling scalar field and decays away as the scalar field approaches the bottom of its potential and picks up speed, similar to how inflation ends in slow-roll inflation. However, to satisfy phenomenological constraints, the potential has to be relatively fine-tuned. But more seriously, recent fits including a full-shape analysis of large-scale structure (LSS) data have challenged the ability of EDE to solve the Hubble tension at all [24–26].

Many of the issues with EDE are avoided in the more recent new early dark energy (NEDE) proposal [27,28]. Here, the early dark energy decays away in a first-order phase transition, and the free energy released is partially converted into small-scale anisotropic stress (behaving similarly to a stiff fluid on large scales) and gravitational radiation, which provides a good fit to all cosmological data, including the recent measurements of H_0 by SH$_0$ES. It remains to be seen, however, what a full-shape analysis of LSS data will imply for NEDE to serve as a new concordance model. The purpose of this short paper is to provide such an analysis.

The full-shape analysis of the matter power spectrum within EDE was carried out in Refs. [25,29] using the

---

[1]A similarly high value was reported based on time delays caused by strong gravitational lenses (H0LiCOW [7]); however, these measurements rely sensitively on assumptions about the mass density profile of elliptical galaxies [8].

effective field theory of large-scale structure[2] (EFTofLSS) applied to BOSS/SDSS data [26,52,53]. In particular, in Ref. [29], the code PyBird was used for the full-shape analysis of LSS data and also made public by the same collaboration. This has enabled us to use the same code to repeat their analysis for NEDE. We therefore employ PyBird to analyze the full-shape of the LSS power spectrum and use it alongside CMB, (small-z and large-z) BAO, and supernovae data to constrain NEDE. We have tested our implementation of it on ΛCDM and wCDM where we find agreement with Refs. [29,54], respectively.

Below, we will provide a short review of the NEDE model, following Refs. [27,28], and then discuss the data analysis and results.

II. NEW EARLY DARK ENERGY

A. Summary of the model

NEDE is associated with the false vacuum energy of a two-component scalar field (ψ, ϕ) that undergoes a first-order phase transition. The corresponding potential reads[3]

$$V(\psi, \phi) = \frac{\lambda}{4}\psi^4 + \frac{1}{2}M^2\psi^2 - \frac{1}{3}\alpha M\psi^3 + \frac{1}{2}m^2\phi^2 + \frac{1}{2}\tilde{\lambda}\phi^2\psi^2,$$

(2.1)

where the parameters λ, $\tilde{\lambda}$, and α are positive and dimensionless, and we assume that $\lambda/\alpha^2 < 1/4$ for the potential to have a nontrivial vacuum structure. In particular, the true vacuum corresponds to $(\psi, \phi)_{\text{True}} = (\frac{M}{2\lambda}[\alpha + \sqrt{\alpha^2 - 4\lambda}], 0)$. With these definitions, the NEDE background energy density at decay time t_* is $\bar{\rho}_{\text{NEDE}}(t_*) = V(\psi_{\text{False}}, \phi(t_*)) - V(\psi_{\text{True}}, 0)$, corresponding to a fraction of the total energy density $\bar{\rho}$ given by $f_{\text{NEDE}} = \bar{\rho}_{\text{NEDE}}(t_*)/\bar{\rho}(t_*)$. The definition of f_{NEDE} does not include the kinetic energy of the fields, which is suppressed before the decay. This additional energy component then leads to an increase in the Hubble parameter $H(t)$, prior to recombination, which in turn reduces the comoving sound horizon $r_s(z_{\text{rec}}) = \int_{z_{\text{rec}}}^{\infty} dz v(z)/H(z)$, with $v(z)$ denoting the sound speed in the photon-baryon fluid. This alone would shift the angular position of the first peak in the CMB power spectrum, $\theta_{\text{rec}} = r_s(z_{\text{rec}})/D_{\text{rec}}$, which is highly constrained. The change in $r_s(z_{\text{rec}})$ is, however, compensated by simultaneously lowering the comoving distance to the surface of last scattering D_{rec}, such that θ_{rec}

remains unchanged. As $D_{\text{rec}} \propto 1/H_0$, this is achieved by an increase in the Hubble parameter H_0, which at the same time resolves the tension between its local and CMB inferred value. For this mechanism to work, it is crucial that the NEDE energy component decays around recombination to avoid overclosing the Universe. In our case, this decay is triggered by the ultralight scalar field $\phi(t)$. It traces an almost flat direction in field space, corresponding to the mass scale $m \sim 10^{-27}$ eV, whereas ψ has a much heavier mass, $M \sim 0.1$ eV $\gg m$, setting the scale of NEDE. This huge hierarchy can be stabilized against quantum corrections by imposing [28] $\tilde{\lambda} < \mathcal{O}(1) \times 10^3 \, m^2/M^2$. Initially, the field is frozen due to the Hubble friction and prevented from tunneling to the true minimum by a high potential barrier in the ψ direction, explicitly $(\psi, \phi)_{\text{ini}} = (0, \phi_{\text{ini}}) \simeq$ const. Once the Hubble drag gets released, ϕ starts rolling, thereby decreasing the potential barrier "seen" by ψ and triggering the phase transition. This happens within one Hubble time and before ϕ reaches its minimum. The exact timing depends on the details of the potential but falls in the range[4] $0.18 < H(t_*)/m < \mathcal{O}(1)$, where the decay time t_* is implicitly determined trough the "trigger parameter" $H(t_*)/m$. The lower bound corresponds to the point of maximal tunneling probability (when ϕ crosses zero for the first time), and the upper bound ensures that the Hubble drag has been released. For $\alpha = \mathcal{O}(1)$, the tunneling rate is $\Gamma(t) \sim M^4 e^{-S_E(t)}$, where $S_E(t)$ is the Euclidian action evaluated at the "bounce solution." Its time dependence is inherited from the trigger field $\phi(t)$ that scans the potential. The inverse duration of the phase transition $\bar{\beta} \simeq \dot{\Gamma}/\Gamma$ (approximating $\Gamma \propto e^{\bar{\beta}t}$) was then found to be [28][5]

$$H(t_*)\bar{\beta}^{-1} = \mathcal{O}(1) \times 10^{-3} \left(\frac{f_{\text{NEDE}}}{0.1}\right)^{1/2} (11\alpha^2/9 - 1)^{-1/2}$$

$$\times \left(\frac{M_{pl}/\phi_{\text{ini}}}{10^4}\right) \left(\frac{H(t_*)/m}{0.2}\right) \left(\frac{\lambda}{0.01}\right)^{3/2}, \quad (2.2)$$

provided $\tilde{\lambda}$ saturates its naturalness bounds and the quartic coupling is sufficiently weak, $\lambda < 0.02$. Here, we used that $S_E(t_*) \simeq 250$, which follows from the percolation condition $\Gamma(t_*)/H^4 \gtrsim 1$. It is fulfilled when bubble nucleation becomes efficient, i.e., there is more than one nucleation event per Hubble time and volume. For the above suggested parameter choices, we therefore find that the phase transition happens on a timescale that is short compared to the

---

[2]The EFTofLSS was first formulated in Refs. [30–32] and later used to compute the dark matter power spectrum [33–45]. An IR-resummed version of the EFTofLSS was then able to reproduce the BAO peak [46–51]. For a more complete account of all related research, see, for example, the references provided in Ref. [26].

[3]As compared to Ref. [28], we have set $\beta = 1$, which can always be achieved by rescaling M. This generic potential has been studied before in an inflationary context in Refs. [55–57].

[4]As argued in Ref. [28], the upper bound tightens to less than or approximately equal to 0.21 when suppressing oscillations of ϕ around the true vacuum.

[5]This expression also controls the amplitude of the gravitational wave signal produced during the phase transition. In Ref. [28], it is argued to be marginally compatible with the peak sensitivity of future pulsar timing arrays in the limit where $H\bar{\beta}^{-1} \to 1$.

Hubble expansion. After the transition, the space is filled with a condensate of colliding bubble walls. This state is dominated by small-scale anisotropic stress and expected to behave on large scales like a fluid dominated by kinetic rather than potential energy, and, therefore, it decays quicker than radiation. As a result, our microscopic model can be described in terms of an effective cosmological fluid, dubbed NEDE fluid, which first (before t_*) behaves like vacuum energy but then (after t_*) redshifts away with an equation-of-state parameter $w_{\mathrm{NEDE}}(t) > 1/3$. In other words, our effective model underlies the assumption that the effect of small-scale nonlinearities can be captured in terms of a cosmic fluid. Ultimately, the fluid parameters such as w_{NEDE} are determined by the microscopic details of our underlying field theory model. A priori, w_{NEDE} is time dependent, but we will approximate it as a constant. This is justified because NEDE can impact cosmological observables only in a short redshift window around its decay time; explicitly, we take

$$w_{\mathrm{NEDE}}(t) = \begin{cases} -1 & \text{for } t < t_*, \\ w_{\mathrm{NEDE}}(t_*) & \text{for } t \geq t_*. \end{cases} \quad (2.3)$$

At the background level, NEDE is therefore described in terms of four parameters, the fraction of NEDE at decay time f_{NEDE}, the mass of the trigger field m, the trigger parameter $H(t_*)/m$ (which together with m fixes the decay redshift z_*), and the equation of state of the NEDE fluid right after percolation has been completed $w_{\mathrm{NEDE}}(t^*)$. The energy density related to the trigger field is always subdominant. As a result, cosmological observables are not sensitive to the initial value of ϕ as long as it is sub-Planckian. Perturbations in the NEDE fluid are generated after the phase transition. They arise from adiabatic perturbations of the trigger field $\delta\phi(t, \mathbf{x})$, which cause spatial variations of the decay time. The NEDE density contrast and velocity divergence as a function of k right after the decay are [28]

$$\delta_{\mathrm{NEDE}}(t_*, k) = -3[1 + w_{\mathrm{NEDE}}(t_*)]H(t_*)\frac{\delta\phi(t_*, k)}{\dot{\phi}(t_*)}, \quad (2.4\mathrm{a})$$

$$\theta_{\mathrm{NEDE}}(t_*, k) = \frac{k^2}{a(t_*)}\frac{\delta\phi(t_*, k)}{\dot{\phi}(t_*)}. \quad (2.4\mathrm{b})$$

These initial values are then propagated forward in time using the adiabatic perturbation equations of a generic fluid [58]. We note that for adiabatic perturbations the matching equations are independent of the initial value of ϕ.[6] This system can be generalized by allowing for a non-vanishing viscosity parameter and a rest-frame sound speed

that deviates from the adiabatic sound speed. These extensions are further investigated in Ref. [28]. Here, we limit the discussion to the simplest case with f_{NEDE} and m as two additional parameters while setting explicitly $w_{\mathrm{NEDE}} = 2/3$.

B. Linear matter power spectrum

The LSS tension is often quantified in terms of the σ_8 parameter, defined as the root-mean-square mass fluctuation within a sphere of radius 8 Mpc/h,

$$\sigma_8^2 = \frac{1}{2\pi^2}\int dk k^2 P(k)[W(k \times 8 \text{ Mpc}/h)]^2, \quad (2.5)$$

where $W(x) = (3/x)[\sin(x)/x^2 - \cos(x)/x]$ is the Fourier transformation of a top-hat window function and $P(k)$ is the matter power spectrum today. In short, the ΛCDM inferred value of σ_8 tends to be too large, leading to a $\simeq 2.5\sigma$ tension when looking at measurements of, say, $S_8 = \sigma_8\sqrt{\Omega_m/0.3}$ (see, for example, Ref. [59] and references in Ref. [60]).

NEDE (as well as other early dark energy models) is known to slightly increase σ_8 and hence not reduce tensions with LSS data when simultaneously fitted to CMB data. To explain this, we first need to understand how NEDE preserves the fit to CMB data (for more details, see the discussion in Refs. [17,28] in the case of acoustic early dark energy and NEDE, respectively). We already stated the main mechanism. Increasing f_{NEDE} lowers the sound horizon $r_s(z_{\mathrm{rec}})$. To keep the corresponding (highly constrained) angular scale θ_{rec} fixed, H_0 needs to be increased. Aside from this background effect, NEDE also manifests itself on the level of perturbations: the decaying NEDE fluid supports its own acoustic oscillations, which, due to their positive pressure, lead to a quicker decay of the gravitational potential that drives CMB oscillations. This potentially dangerous effect can then be reversed by increasing the cold dark matter density through ω_{cdm}. Moreover, the background modification leads to a reduction of the CMB damping scale, which needs to be countered by increasing both the amplitude A_s and tilt n_s of the primordial power spectrum. While all these effects can be balanced in a way which leaves the CMB power spectrum approximately invariant, this is not exactly true for the matter power spectrum.

This is illustrated in Fig. 1(a), where we vary different model parameters to study their impact on the *linear* matter power spectrum (relative to the best-fit cosmology in the third column of Table I). The relative changes are chosen such that the accumulated effect of all parameter changes on the CMB power spectrum is approximately vanishing.[7] Moreover, to account for the main degeneracy between f_{NEDE} and H_0, we kept θ_{rec} fixed in all plots by dialing the

---

[6]A more detailed discussion of this point is provided within the methodology part of Ref. [28].

[7]This is illustrated explicitly in Fig. 9 in Ref. [28] for the same parameter choices.
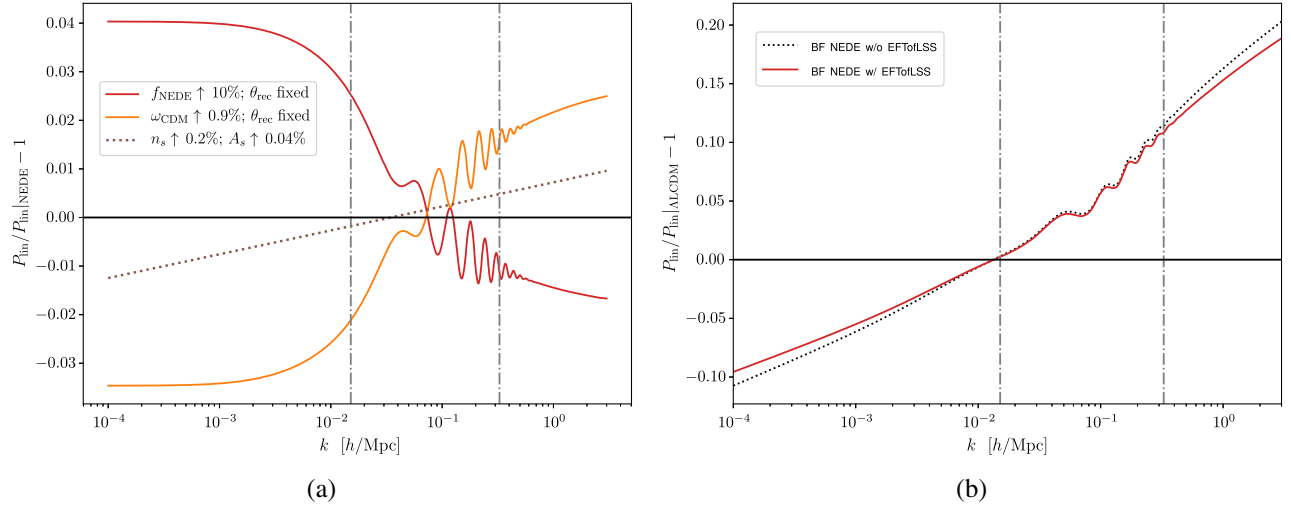
FIG. 1. Relative change of the linear matter power spectrum. Best-fit (BF) values are taken from Table I. The k range between the vertical dot-dashed lines makes an approximate 90% contribution to the σ_8 integral (2.5) (when evaluated for $P_{\rm lin}$). Generically, NEDE leads to less power on large and more power on small scales, causing a small net increase in σ_8. (a) Eect of varying dierent NEDE parameters and (b) Comparison between bestt CDM and NEDE.

TABLE I. The mean value and $\pm 1\sigma$ error (with best-fit value in parentheses) of the cosmological parameters from our combined analyses for ΛCDM and NEDE with and without EFTofLSS.

Parameter	ΛCDM		NEDE	
	w/o EFTofLSS	w/EFTofLSS	w/o EFTofLSS	w/EFTofLSS
$100\,\omega_b$	$2.251^{+0.014}_{-0.013}$ (2.251)	$2.250^{+0.013}_{-0.014}$ (2.256)	$2.292^{+0.022}_{-0.024}$ (2.297)	$2.290^{+0.022}_{-0.023}$ (2.288)
ω_{cdm}	$0.1184^{+0.0009}_{-0.0009}$ (0.1183)	$0.1183^{+0.0009}_{-0.0009}$ (0.1181)	$0.1304^{+0.0034}_{-0.0035}$ (0.1306)	$0.1291^{+0.0033}_{-0.0034}$ (0.1295)
H_0(kms^{-1} Mpc^{-1})	$68.13^{+0.41}_{-0.41}$ (68.16)	$68.14^{+0.40}_{-0.41}$ (68.31)	$71.4^{+1.0}_{-1.0}$ (71.5)	$71.2^{+1.0}_{-1.0}$ (71.28)
$ln 10^{10}A_s$	$3.053^{+0.014}_{-0.016}$ (3.053)	$3.051^{+0.014}_{-0.015}$ (3.049)	$3.067^{+0.014}_{-0.015}$ (3.068)	$3.065^{+0.014}_{-0.015}$ (3.064)
n_s	$0.9686^{+0.0037}_{-0.0037}$ (0.9698)	$0.9686^{+0.0037}_{-0.0037}$ (0.9696)	$0.9889^{+0.0067}_{-0.0066}$ (0.9912)	$0.9876^{+0.0070}_{-0.0066}$ (0.9884)
τ_{reio}	$0.0599^{+0.0071}_{-0.0078}$ (0.0598)	$0.0589^{+0.0068}_{-0.0078}$ (0.0573)	$0.0571^{+0.0068}_{-0.0077}$ (0.0572)	$0.0571^{+0.0068}_{-0.0077}$ (0.0557)
$f_{\rm NEDE}$	$\cdots$	$\cdots$	$0.126^{+0.032}_{-0.029}$ (0.1296)	$0.117^{+0.033}_{-0.030}$ (0.120)
$\log_{10}(m/m_0)$	$\cdots$	$\cdots$	$2.56^{+0.12}_{-0.10}$ (2.57)	$2.55^{+0.12}_{-0.11}$ (2.53)
σ_8	$0.8090^{+0.0060}_{-0.0065}$ (0.8092)	$0.8080^{+0.0058}_{-0.0063}$ (0.8064)	$0.839^{+0.010}_{-0.010}$ (0.841)	$0.836^{+0.010}_{-0.010}$ (0.837)
S_8	$0.814^{+0.010}_{-0.010}$	$0.813^{+0.010}_{-0.010}$	$0.841^{+0.012}_{-0.012}$	$0.836^{+0.012}_{-0.012}$
r_s^d (Mpc)	$147.40^{+0.23}_{-0.23}$ (147.38)	$147.40^{+0.23}_{-0.23}$ (147.39)	$141.0^{+1.6}_{-1.7}$ (140.9)	$141.6^{+1.6}_{-1.7}$ (141.4)
z_*	$\cdots$	$\cdots$	4920^{+620}_{-730} (4960)	4900^{+660}_{-800} (4720)
$\Delta\chi^2$	0	0	-15.6	-14.7
$f_{\rm NEDE} \neq 0$	$\cdots$	$\cdots$	4.3σ	3.9σ
$10^3 \times \max(R-1)$	2.1	2.7	7.8	3.3

value of H_0 correspondingly. To keep the discussion simple, we focus on scales that give the dominant contribution (90%) to the σ_8 integral in (2.5) and are demarcated by the dot-dashed lines.[8] First, the red line

shows the effect of a 10% increase in $f_{\rm NEDE}$. This leads to a loss of power on small scales, which, again, can be attributed to the quicker decay of the gravitational potential. Now, the CMB fit can be preserved by increasing $\omega_{\rm cdm}$ (by $\simeq 0.9\%$, yellow line), A_s (by $\simeq 0.04\%$, dotted purple line), and n_s (by $\simeq 0.2\%$, dotted purple line). However, we see that this cancellation does not work quite as perfectly in the case

---

[8]On larger scales, the main effect is caused by changes to the background evolution.

of the matter power spectrum. Instead, the additional power due to the increase in cold dark matter and primordial power overcompensates the depressing effect of f_{NEDE}, leaving us with slightly more power on BAO scales (and less power on larger scales). This is also shown in the right panel when comparing our NEDE best-fit cosmology with ΛCDM: NEDE is changing the shape of the linear power spectrum by tilting it. As a side effect, there is more power on scales that were subhorizon by the time of matter-radiation equality, leading to a small increase in σ_8 through (2.5). This discussion also shows that LSS data are going to be a challenge for NEDE. We will therefore assess its constraining power in the next section by applying the EFTofLSS to BOSS/SDDS data. This analysis probes changes in the shape of the power spectrum on BAO scales and hence should be affected by the observed tilting.

III. DATA ANALYSIS AND RESULTS

We use the publicly available code TriggerCLASS[9] [28], which implements NEDE in the Boltzmann code CLASS (Cosmic Linear Anisotropic Solving System) [62]. We then scan the cosmological parameters with the Monte Carlo Markov chain (MCMC) code MontePython [63,64], employing the Metropolis-Hastings algorithm. To that end, we impose flat priors with standard ranges on the dimensionless baryon and cold dark matter density, ω_b and ω_{cdm}; the Hubble parameter H_0; the amplitude of primordial curvature perturbations at $k = 0.05 \text{ Mpc}^{-1}$, $\ln 10^{10} A_s$; the spectral tilt n_s; and the reionization optical depth τ_{reio}. In keeping with the Planck convention, the neutrino sector contains two massless and one massive species with $M_\nu = 0.06$ eV, where the effective number of relativistic degrees of freedom is fixed to $N_{\text{eff}} = 3.046$. Alongside these standard parameters, we also vary the trigger mass through $\log_{10}(m/m_0)$ (where $m_0 = 1/\text{Mpc}$) and the NEDE fraction f_{NEDE}. We impose flat priors with ranges $1.3 < \log_{10}(m/m_0) < 3.3$ and $0 < f_{\text{NEDE}} < 0.3$. ΛCDM is recovered for $f_{\text{NEDE}} = 0$. For our base model, we further fix $H(t_*)/m = 0.2$ in accordance with our theoretical discussion. We also set $w_{\text{NEDE}}(t_*) = 2/3$ corresponding to an initial admixture of a stiff fluid.[10] The perturbation sector assumes a rest-frame sound speed that equals the adiabatic sound speed and a vanishing viscosity parameter (as defined in Ref. [65]). To summarize, we study a two-parameter extension of ΛCDM with flat parameter priors.

In all our runs, we include the following datasets: the Planck 2018 TT, TE, EE, and lensing likelihood with the full set of nuisance parameters [66]; supernovae data from the combined Pantheon sample [67]; the locally measured value $H_0 = 74.03 \pm 1.42 \text{ km s}^{-1} \text{ Mpc}^{-1}$ (68% C.L.) from SH$_0$ES [1] implemented as a Gaussian prior; the primordial

Helium abundance $Y_p = 0.2449 \pm 0.0040$ (68% C.L.) from Ref. [68]; and the small-z BAO measurements of the SDDS DR7 main Galaxy sample [69] and the 6dF Galaxy Survey [70] at redshifts $z = 0.15$ and $z = 0.106$, respectively. With regard to any additional dataset, we distinguish two different analyses:

(1) Combined analysis *without EFTofLSS*: high-z BAO measurements together with constraints on $f\sigma_8$, quantifying the growth of structure, obtained from the CMASS and LOWZ galaxy samples of BOSS DR 12 [71] at redshifts $z = 0.38, 0.51, 0.61$. This run does not capture the full shape of the matter power spectrum (it merely contains some condensed information through $f\sigma_8$).

(2) Combined analysis *with EFTofLSS*: here, we include the EFTofLSS applied to the BOSS/SDDS sample [26,52,53]. It contains the full-shape information on the galaxy power spectra obtained from the sky cuts CMASS NGC, CMASS SGC, and LOWZ NGC at the effective redshifts $z = 0.57$ (CMASS) and $z = 0.32$ (LOWZ). This is combined with constraints on BAO parameters measured from the same samples using the postreconstructed power spectra and taking into account the covariance among all datasets. The full-shape and BAO data together with their covariances are implemented via the MontePython likelihood extension PyBird.[11] We impose the same priors on the eight EFT parameters as the ones in Ref. [54], including a flat prior on the linear galaxy bias b_1.

For each dataset combination, we run both the ΛCDM and our NEDE base model using between 8 and 16 chains. We consider chains to be converged if the Gelman-Rubin criterion [73] fulfills $R - 1 < 0.01$. Especially in the case of NEDE, this requires a rather large number of total steps of the order 3×10^6. As we find, this is vital to deriving well-converged uncertainties for f_{NEDE}, needed to make a reliable statement about the statistical evidence for NEDE. The exact convergence values are detailed in Table I. For initial covariance matrices, we use the ones from the respective ΛCDM runs, which are then updated through MontePython's "superupdate" option. We also tested our data pipeline, including its PyBird implementation, by reproducing different results obtained in Ref. [54] in the case of wCDM.[12]

A detailed discussion of NEDE and its phenomenology has been provided in Ref. [28]. Here, we will therefore limit ourselves to a quick review of the main phenomenological features of NEDE and rather focus on the impact additional LSS data has on the extracted parameter values. As

---

[9]See Ref. [61].
[10]For extended runs where either parameter is allowed to vary, see Ref. [28].

[11]See Ref. [72].
[12]Specifically, we checked that we agree with the results of the MCMC analyses performed with the dataset combinations BAO + FS, BAO + FS w/o Ly-α, CMB + BAO, and CMB + FS + BAO.
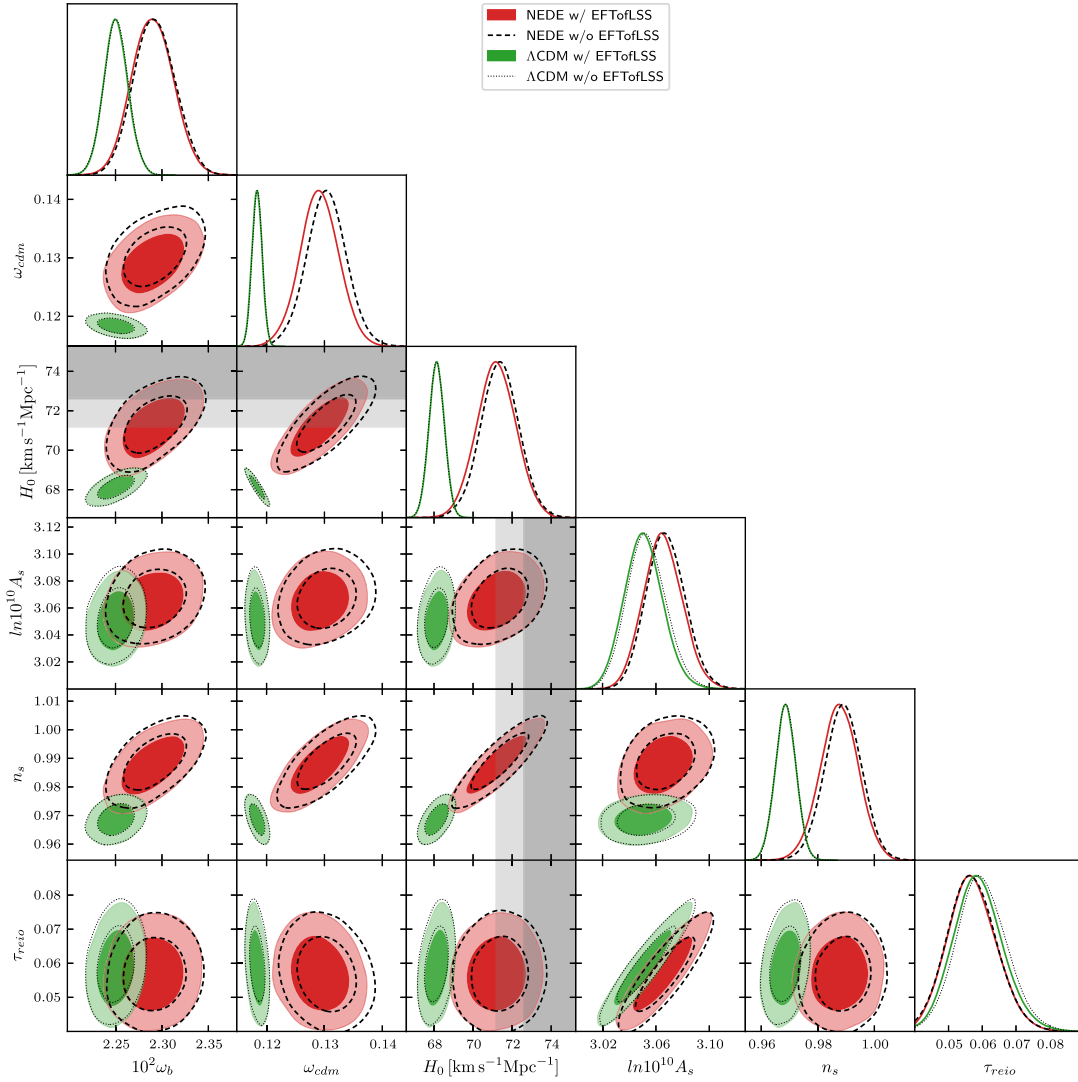
FIG. 2. Posteriors and covariances of standard cosmological parameters for ΛCDM (green) and NEDE (red). The result of the combined analysis without EFTofLSS corresponds to the dashed (NEDE) and dotted (ΛCDM) contours. Here and henceforth, the 68% C.L. and the 95% C.L. correspond to the darker and lighter shaded regions, respectively. The gray band corresponds to the SH_0ES constraint on H_0. Overall, including EFTofLSS has a negligible effect.

mentioned before, the primary effect of NEDE is to lower the sound horizon, which is balanced by increasing H_0. This can be seen in Fig. 3, which shows an (approximate) degeneracy between H_0 and the sound horizon at radiation drag r_s^d. As a result, the NEDE contour (with and without EFTofLSS) largely overlaps with the gray band representing the SH_0ES measurement, thereby resolving the Hubble tension. Another crucial effect of NEDE, especially relevant for LSS, is its positive correlation with the (dimensionless) dark matter energy density ω_{cdm}, as explained through Fig. 1(a). This can, for example, be seen in the H_0 vs w_{cdm} plot in Fig. 2. Finally, the enhanced diffusion damping on small scales is counteracted by a reduced spectral tilt (or $n_s \to 1$ equivalently). Specifically, from Fig. 2, we infer that n_s becomes 2σ compatible with a scale invariant spectrum.

Here, we ask whether this picture is adversely affected by including additional LSS data as recently claimed in the context of the old EDE proposal [25,29]. The short answer is that this is not the case. Including additional LSS data only leads to an insignificant change of previous results without the EFTofLSS dataset. This is obvious from comparing the red (with EFTofLSS) and dashed contours (without EFTofLSS) in Figs. 2 and 3, which are almost identical. On a more quantitative level, we report a small reduction of the preferred amount of NEDE as detailed in Table I. Without including the EFTofLSS, we have $f_{NEDE} = 12.6^{+3.2}_{-2.9}\%$, which corresponds to a 4.3σ evidence for a nonvanishing NEDE parameter and an increased Hubble parameter of $H_0 = 71.4 \pm 1.0 \text{ km s}^{-1} \text{Mpc}^{-1}$. These values undergo small insignificant ($<0.5\sigma$) changes when we include the EFTofLSS, specifically
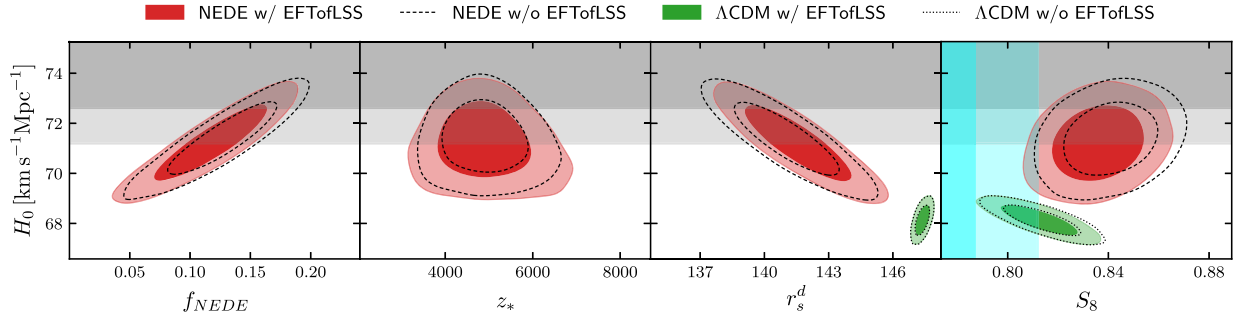
FIG. 3. Covariances of H_0 vs a subset of parameters for the combined analysis with (red and green filled contour) and without (dashed and dotted contour) EFTofLSS. A recent constraint on S_8 from weak gravitational lensing [59] is depicted by the light blue band. The gray band represents the recent SH$_0$ES measurement. The change in $f_{\rm NEDE}$ when including EFTofLSS is insignificant.

TABLE II. The best fit $\chi^2 = -2\ln(\mathcal{L})$ from combined analysis with and without EFTofLSS. The relative fit improvement is quantified through $\Delta\chi^2 = \chi^2(\text{NEDE}) - \chi^2(\Lambda\text{CDM})$.

Dataset	ΛCDM		NEDE			
EFTofLSS + BAO	w/o	w/	w/o		w/	
	χ^2	χ^2	χ^2	$\Delta\chi^2$	χ^2	$\Delta\chi^2$
Planck high-ℓ TT, TE, EE	2,348.9	2351.1	2,348.2	-0.8	2348.2	-2.9
Planck low-ℓ TT	22.7	22.6	20.8	-1.9	21.0	-1.6
Planck low-ℓ EE	397.3	396.5	396.4	-0.9	396.1	-0.4
Planck lensing	9.1	9.6	9.5	0.4	9.4	-0.2
BAO low-z	1.6	1.8	1.8	0.1	1.8	0.1
BAO high-z + $f\sigma_8$	5.9	$\cdots$	6.8	0.9	$\cdots$	$\cdots$
EFTofLSS + BAO/CMASS NGC	$\cdots$	65.9	$\cdots$	$\cdots$	67.1	1.3
EFTofLSS + BAO/CMASS SGC	$\cdots$	61.9	$\cdots$	$\cdots$	63.0	1.1
EFTofLSS + BAO/LOWZ NGC	$\cdots$	69.9	$\cdots$	$\cdots$	69.9	0.0
Pantheon	1,027.0	1026.9	1,027.3	0.3	1027.4	0.5
BBN	< 0.1	< 0.1	< 0.1	0.0	< 0.1	0.0
SH$_0$ES	17.1	16.2	3.3	-13.8	3.7	-12.5
χ^2(total)	3,829.6	4,022.5	3,814.0	$\cdots$	4,007.8	$\cdots$
$\Delta\chi^2$(total)	$\cdots$	$\cdots$	$\cdots$	-15.6	$\cdots$	-14.7

$f_{\rm NEDE} = 11.7^{+3.3}_{-3.0}\%$ and $H_0 = 71.2 \pm 1.0 \text{ km s}^{-1}\,\text{Mpc}^{-1}$, corresponding to a (still large) 3.9σ evidence for NEDE. With regard to the standard ΛCDM parameters, the biggest change occurs for $w_{\rm cdm}$, which decreases by 1%, whereas the other ΛCDM parameters change by less than 0.3%. This had to be expected as $\omega_{\rm cdm}$ directly affects LSS parameters and hence is most constrained by the EFTofLSS. Moreover, as argued in Sec. II B, decreasing $w_{\rm cdm}$, while keeping the other parameters approximately constant, leads to a slight decrease in the σ_8 parameter. This in turn reduces $S_8 = \sigma_8\sqrt{\Omega_m/0.3}$ by 0.6% (the effect is attenuated by a slight drop in H_0). The phenomenological constraints are depicted as the light blue band in the last panel of Fig. 3 (we cite $S_8 = 0.762^{+0.025}_{-0.024}$ from a combined tomographic weak gravitational lensing analysis of the Kilo Degree Survey and the Dark Energy Survey [59]). We then find that the S_8 tension is still significant at 2.7σ (and 2.8σ without EFTofLSS). However, this has to be compared to a

$\simeq 2.5\sigma$ tension within ΛCDM [28,59] (without SH$_0$ES),[13] which is only marginally lower.

This picture is confirmed by our χ^2 analysis in Table II. It shows that the overall χ^2 improvement is only slightly affected by including the EFTofLSS and amounts to $\Delta\chi^2$(total) $\simeq -15$. In this context, it is interesting to note that the ΛCDM fit to high-ℓ Planck data gets worse upon inclusion of the EFTofLSS data, which we believe is a manifestation of the LSS/S_8 tension already present within ΛCDM at the $\simeq 2$–3σ level [59,74]. Within NEDE, on the other hand, that deterioration of the high-ℓ Planck fit can be completely avoided. We attribute this to the tendency of NEDE to give less power on small scales, which is a distinctive feature when comparing with its EDE competitors

---

[13]Note that including SH$_0$ES lowers the tension within ΛCDM. This, however, is not a viable way of alleviating the problem as it relies on combining incompatible datasets.
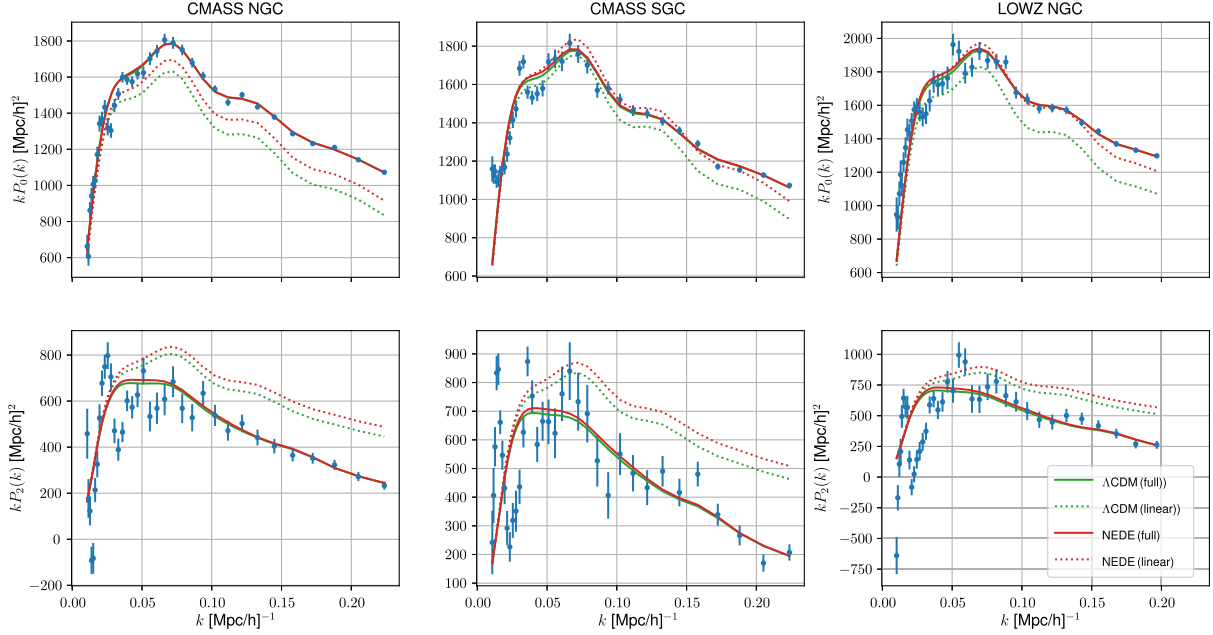
FIG. 4.   Monopole (first row) and quadrupole (second row) of the EFT-corrected redshift-space power spectrum for all three sky cuts. The green and red curves correspond, respectively, to the ΛCDM and NEDE best-fit cosmology with the EFTofLSS as detailed in Table I. The dotted line is the contribution from the linear power spectrum. In agreement with our χ^2 comparison in Table II, ΛCDM and NEDE provide similarly good fits.

and ΛCDM (see Fig. 17 in Ref. [28]). This, however, comes at the price of worsening the fit to the EFTofLSS dataset. Both effects—the improved fit to Planck and the worse fit to the full-shape data—compensate each other almost perfectly. In other words, the additional LSS data lead to a similar overall (negative) effect on both the ΛCDM and NEDE fit, which explains why it cannot significantly lower the evidence for NEDE.

Finally, we plotted the best-fit monopole ($\ell = 0$) and quadrupole ($\ell = 2$) of the EFT-corrected redshift space power spectrum in Fig. 4. More explicitly, they are obtained from

$$P_\ell^{(\text{true})}(q) = \frac{2\ell + 1}{2} \int_{-1}^{1} d\mu P(q, \mu) \mathcal{L}_\ell(\mu), \qquad (3.1)$$

after applying the Alcock-Paczynski transformation to account for the fact that the observation uses a fictitious cosmology to convert redshifts and celestial coordinates to Cartesian coordinates. Here, $\mu = \mathbf{k} \cdot \hat{\mathbf{z}}/k$ with $\hat{\mathbf{z}}$ being the line-of-sight unit vector, $\mathcal{L}_\ell$ is the Legendre polynomials, and $P(q, \mu)$ is the redshift-space power spectrum at one-loop order. Its expression in terms of EFT parameters can be found, for example, in the Appendix of Ref. [54] alongside the explicit Alcock-Paczynski transformation relating $\{q, P_\ell^{(\text{true})}(q)\}$ with $\{k, P_\ell(k)\}$. To provide an explicit example, the linear contribution to $P(q, \mu)$, giving rise to the dotted lines in Fig. 4, is given by

$$P_{\text{lin}}(q, \mu) = (b_1 + f\mu^2)^2 P_{\text{lin}}(q), \qquad (3.2)$$

where f is the linear growth rate, $P_{\text{lin}}(q)$ is the linear power spectrum at a given redshift, and b_1 is the linear galaxy bias,

which we fitted for each sky cut separately. Again, the crucial observation is that both NEDE and ΛCDM fit the full shape of the power spectrum equally well. Moreover, in agreement with Fig. 1(b), we see that the linear spectrum predicts more power on short scales for NEDE due to the relative tilting we observed before. This difference, however, is absent in the loop-corrected expressions. In other words, the EFT corrections act in favor of NEDE. This discussion also shows that the scatter and error in the data are still too large to discriminate between the tiny shape difference between the ΛCDM and NEDE spectrum.

IV. CONCLUSIONS

In this short paper, we confronted NEDE with full-shape LSS data using the EFTofLSS applied to BOSS/SDSS in order to address recent concerns regarding the phenomenological viability of a class of EDE models. To that end, we used the publicly available code PyBird, which allowed us to implement the same data pipeline as the one used in Ref. [26] to constrain single-field EDE models.[14] We report that adding the full-shape information has an insignificant effect on NEDE. In particular, we still find a rather high

---

[14]This work does not include direct constraints on S_8 from photometric surveys to retain comparability with the PyBird analysis of EDE in Ref. [26]. We intend to study the effect of further LSS constraints in our future work when looking at extensions of NEDE that can alleviate the LSS tension. In contrast to the EFTofLSS analysis, which takes the linear power spectrum as input, this requires explicit N-body simulations to test the accuracy of semianalytic methods like HaloFit [75] or HMcode [76].

$\simeq 4\sigma$ evidence for a nonvanishing fraction of NEDE alongside $H_0 = 71.2 \pm 1.0$ km s^{-1} Mpc^{-1} (68% C.L.), which is fully compatible with $H_0 = 71.4 \pm 1.0$ km s^{-1} Mpc^{-1} (68% C.L.) obtained without full-shape data. In conclusion, our model is consistent with current LSS data as implemented by PyBird.

However, it is also clear from our analysis that NEDE cannot improve on the tension with LSS data already present in ΛCDM. In particular, NEDE is 2.7σ discrepant with the value of S_8, which is of a similar level as the tension within ΛCDM. There are two main conclusions we can reach from this. First, more LSS data, as they are provided by present and future spectroscopic galaxy surveys such as Euclid [77] and the Dark Energy Spectroscopic Instrument [78], have the potential to confirm or rule out the base NEDE model as a resolution to the Hubble tension. A similar point was made in the case of single-field EDE [25]. Second, further improvements of the current model should be guided by the aim to reduce the S_8 tension below its ΛCDM level. For different ideas of how this can be achieved within NEDE see the corresponding discussion in Ref. [28].

Finally, we have limited the discussion here to the base NEDE model for simplicity. A more extensive LSS analysis which allows the fluid parameters to vary freely might provide additional freedom needed to better accommodate LSS data.

ACKNOWLEDGMENTS

[1] A. G. Riess, S. Casertano, W. Yuan, L. M. Macri, and D. Scolnic, Astrophys. J. **876**, 85 (2019).

[2] N. Aghanim *et al.* (Planck Collaboration), Astron. Astrophys. **641**, A6 (2020).

[3] J. L. Bernal, L. Verde, and A. G. Riess, J. Cosmol. Astropart. Phys. 10 (2016) 019.

[4] L. Knox and M. Millea, Phys. Rev. D **101**, 043533 (2020).

[5] L. Verde, T. Treu, and A. Riess, Nat. Astron. **3**, 891 (2019).

[6] A. G. Riess, Nat. Rev. Phys. **2**, 10 (2020).

[7] K. C. Wong *et al.*, Mon. Not. R. Astron. Soc. **498**, 1420 (2020).

[8] S. Birrer *et al.*, Astron. Astrophys. **643**, A165 (2020).

[9] W. L. Freedman *et al.*, arXiv:1907.05922.

[10] W. L. Freedman, B. F. Madore, T. Hoyt, I. S. Jang, R. Beaton, M. G. Lee, A. Monson, J. Neeley, and J. Rich, arXiv:2002.01550.

[11] K. Aylor, M. Joy, L. Knox, M. Millea, S. Raghunathan, and W. L. K. Wu, Astrophys. J. **874**, 4 (2019).

[12] L. Verde, J. L. Bernal, A. F. Heavens, and R. Jimenez, Mon. Not. R. Astron. Soc. **467**, 731 (2017).

[13] N. Arendse, A. Agnello, and R. Wojtak, Astron. Astrophys. **632**, A91 (2019).

[14] V. Poulin, T. L. Smith, D. Grin, T. Karwal, and M. Kamionkowski, Phys. Rev. D **98**, 083525 (2018).

[15] V. Poulin, T. L. Smith, T. Karwal, and M. Kamionkowski, Phys. Rev. Lett. **122**, 221301 (2019).

[16] T. L. Smith, V. Poulin, and M. A. Amin, Phys. Rev. D **101**, 063523 (2020).

[17] M.-X. Lin, G. Benevento, W. Hu, and M. Raveri, Phys. Rev. D **100**, 063542 (2019).

[18] N. Kaloper, Int. J. Mod. Phys. D **28**, 1944017 (2019).

[19] S. Alexander and E. McDonough, Phys. Lett. B **797**, 134830 (2019).

[20] E. Hardy and S. Parameswaran, Phys. Rev. D **101**, 023503 (2020).

[21] J. Sakstein and M. Trodden, Phys. Rev. Lett. **124**, 161301 (2020).

[22] M. Braglia, W. T. Emond, F. Finelli, A. E. Gumrukcuoglu, and K. Koyama, Phys. Rev. D **102**, 083513 (2020).

[23] M. Gonzalez, M. P. Hertzberg, and F. Rompineve, J. Cosmol. Astropart. Phys. 10 (2020) 028.

[24] J. C. Hill, E. McDonough, M. W. Toomey, and S. Alexander, Phys. Rev. D **102**, 043507 (2020).

[25] M. M. Ivanov, E. McDonough, J. C. Hill, M. Simonović, M. W. Toomey, S. Alexander, and M. Zaldarriaga, Phys. Rev. D **102**, 103502 (2020).

[26] G. D'Amico, J. Gleyzes, N. Kokron, K. Markovic, L. Senatore, P. Zhang, F. Beutler, and H. Gil-Marín, J. Cosmol. Astropart. Phys. 05 (2020) 005.

[27] F. Niedermann and M. S. Sloth, Phys. Rev. D **103**, L041303 (2021).

[28] F. Niedermann and M. S. Sloth, Phys. Rev. D **102**, 063527 (2020).

[29] G. D'Amico, L. Senatore, P. Zhang, and H. Zheng, arXiv:2006.12420.

[30] D. Baumann, A. Nicolis, L. Senatore, and M. Zaldarriaga, J. Cosmol. Astropart. Phys. 07 (2012) 051.

[31] J. J. M. Carrasco, M. P. Hertzberg, and L. Senatore, J. High Energy Phys. 09 (2012) 082.

[32] R. A. Porto, L. Senatore, and M. Zaldarriaga, J. Cosmol. Astropart. Phys. 05 (2014) 022.

[33] J. J. M. Carrasco, S. Foreman, D. Green, and L. Senatore, J. Cosmol. Astropart. Phys. 07 (2014) 056.

[34] J. J. M. Carrasco, S. Foreman, D. Green, and L. Senatore, J. Cosmol. Astropart. Phys. 07 (2014) 057.

[35] S. M. Carroll, S. Leichenauer, and J. Pollack, Phys. Rev. D **90**, 023518 (2014).

[36] L. Senatore and M. Zaldarriaga, J. Cosmol. Astropart. Phys. 02 (2015) 013.
[37] T. Baldauf, E. Schaan, and M. Zaldarriaga, J. Cosmol. Astropart. Phys. 03 (2016) 007.
[38] S. Foreman, H. Perrier, and L. Senatore, J. Cosmol. Astropart. Phys. 05 (2016) 027.
[39] T. Baldauf, L. Mercolli, and M. Zaldarriaga, Phys. Rev. D **92,** 123007 (2015).
[40] M. Cataneo, S. Foreman, and L. Senatore, J. Cosmol. Astropart. Phys. 04 (2017) 026.
[41] M. Lewandowski and L. Senatore, J. Cosmol. Astropart. Phys. 08 (2017) 037.
[42] T. Konstandin, R. A. Porto, and H. Rubira, J. Cosmol. Astropart. Phys. 11 (2019) 027.
[43] E. Pajer and M. Zaldarriaga, J. Cosmol. Astropart. Phys. 08 (2013) 037.
[44] A. A. Abolhasani, M. Mirbabayi, and E. Pajer, J. Cosmol. Astropart. Phys. 05 (2016) 063.
[45] L. Mercolli and E. Pajer, J. Cosmol. Astropart. Phys. 03 (2014) 006.
[46] L. Senatore and M. Zaldarriaga, arXiv:1409.1225.
[47] M. Lewandowski, A. Perko, and L. Senatore, J. Cosmol. Astropart. Phys. 05 (2015) 019.
[48] T. Baldauf, M. Mirbabayi, M. Simonović, and M. Zaldarriaga, Phys. Rev. D **92,** 043514 (2015).
[49] D. Blas, M. Garny, M. M. Ivanov, and S. Sibiryakov, J. Cosmol. Astropart. Phys. 07 (2016) 028.
[50] L. Senatore and G. Trevisan, J. Cosmol. Astropart. Phys. 05 (2018) 019.
[51] M. Lewandowski and L. Senatore, J. Cosmol. Astropart. Phys. 03 (2020) 018.
[52] M. M. Ivanov, M. Simonović, and M. Zaldarriaga, J. Cosmol. Astropart. Phys. 05 (2020) 042.
[53] T. Colas, G. D'amico, L. Senatore, P. Zhang, and F. Beutler, J. Cosmol. Astropart. Phys. 06 (2020) 001.
[54] G. D'Amico, L. Senatore, and P. Zhang, J. Cosmol. Astropart. Phys. 01 (2021) 006.
[55] A. D. Linde, Phys. Lett. B **249,** 18 (1990).
[56] F. C. Adams and K. Freese, Phys. Rev. D **43,** 353 (1991).
[57] E. J. Copeland, A. R. Liddle, D. H. Lyth, E. D. Stewart, and D. Wands, Phys. Rev. D **49,** 6410 (1994).
[58] C.-P. Ma and E. Bertschinger, Astrophys. J. **455,** 7 (1995).
[59] S. Joudaki et al., Astron. Astrophys. **638,** L1 (2020).
[60] E. Di Valentino et al., arXiv:2008.11285.
[61] https://github.com/flo1984/TriggerCLASS.
[62] D. Blas, J. Lesgourgues, and T. Tram, J. Cosmol. Astropart. Phys. 07 (2011) 034.
[63] B. Audren, J. Lesgourgues, K. Benabed, and S. Prunet, J. Cosmol. Astropart. Phys. 02 (2013) 001.
[64] T. Brinckmann and J. Lesgourgues, Phys. Dark Universe **24,** 100260 (2019).
[65] W. Hu, Astrophys. J. **506,** 485 (1998).
[66] N. Aghanim et al. (Planck Collaboration), Astron. Astrophys. **641,** A5 (2020).
[67] D. M. Scolnic et al., Astrophys. J. **859,** 101 (2018).
[68] E. Aver, K. A. Olive, and E. D. Skillman, J. Cosmol. Astropart. Phys. 07 (2015) 011.
[69] A. J. Ross, L. Samushia, C. Howlett, W. J. Percival, A. Burden, and M. Manera, Mon. Not. R. Astron. Soc. **449,** 835 (2015).
[70] F. Beutler, C. Blake, M. Colless, D. H. Jones, L. Staveley-Smith, L. Campbell, Q. Parker, W. Saunders, and F. Watson, Mon. Not. R. Astron. Soc. **416,** 3017 (2011).
[71] S. Alam et al. (BOSS Collaboration), Mon. Not. R. Astron. Soc. **470,** 2617 (2017).
[72] https://github.com/pierrexyz/pybird.git.
[73] A. Gelman and D. B. Rubin, Stat. Sci. **7,** 457 (1992).
[74] M. Asgari et al., Astron. Astrophys. **634,** A127 (2020).
[75] R. E. Smith, J. A. Peacock, A. Jenkins, S. D. M. White, C. S. Frenk, F. R. Pearce, P. A. Thomas, G. Efstathiou, and H. M. P. Couchmann (VIRGO Consortium Collaboration), Mon. Not. R. Astron. Soc. **341,** 1311 (2003).
[76] A. Mead, J. Peacock, C. Heymans, S. Joudaki, and A. Heavens, Mon. Not. R. Astron. Soc. **454,** 1958 (2015).
[77] L. Amendola et al., Living Rev. Relativity **21,** 2 (2018).
[78] M. E. Levi et al. (DESI Collaboration), arXiv:1907.10688.